

## Infrared and Raman studies of the Verwey transition in magnetite

L. V. Gasparov and D. B. Tanner

*University of Florida, Department of Physics, P.O. Box 118440, Gainesville Florida 32611-8440*

D. B. Romero

*NIST-Optical Technology Division, Gaithersburg, Maryland 20899-8441*

*and Physics Department, University of Maryland, College Park, Maryland 20742*

H. Berger and G. Margaritondo

*Physics Department-IPA, École Polytechnique Fédéral de Lausanne, CH-1015 Lausanne, Switzerland*

L. Forró

*Physics Department-IGA, École Polytechnique Fédéral de Lausanne, CH-1015 Lausanne, Switzerland*

(Received 17 May 1999; revised manuscript received 7 March 2000)

We present infrared and Raman measurements of magnetite ( $\text{Fe}_3\text{O}_4$ ). This material is known to undergo a metal-insulator and a structural transition (Verwey transition) at  $T_V=120$  K. The structural aspect of the Verwey transition is disclosed by the appearance of additional infrared-active and Raman-active phonons. The frequencies of the infrared-active phonons show no significant singularities at the transition whereas their linewidths increase. The frequency and linewidth of the Raman-active phonon at  $670\text{ cm}^{-1}$  change abruptly at the transition. For  $T < T_V$ , we observe fine structure in the infrared and Raman spectra which may indicate strong anharmonicity of the system below the transition. The effective mass of the mobile carriers is estimated to be  $m^* \approx 100m$ , where  $m$  is the electronic mass.

### I. INTRODUCTION

#### A. The Verwey transition

Charge ordering in strongly correlated electron systems has recently attracted a lot of attention on account of its influence on charge transport and dynamics. In the high-temperature superconductors, there is evidence of the formation of charge and spin stripes near the commensurate doping  $x = \frac{1}{8}$  in  $\text{La}_{2-x}\text{Sr}_x\text{CuO}_4$  in which superconductivity is suppressed.<sup>1</sup> The suppression was attributed to the pinning by lattice distortions of the dynamic charge and spin stripes formed in this phase.<sup>1,2</sup> Very recently, Raman scattering in the  $\text{NaV}_2\text{O}_5$  compound revealed considerable charge ordering below  $T \approx 35$  K.<sup>3</sup> In the manganates, charge ordering is observed at certain commensurate doping values.<sup>4</sup> The possibility of the coexistence of ferromagnetic and charge-order correlations may be relevant in understanding the phenomenon of colossal magnetoresistance in manganates.

The earliest compound known<sup>5</sup> to manifest charge ordering is magnetite ( $\text{Fe}_3\text{O}_4$ ).  $\text{Fe}_3\text{O}_4$  is a ferrimagnet below 850 K. At room temperature,  $\text{Fe}_3\text{O}_4$  has an inverse spinel cubic structure with the  $O_h^7 (Fd3m)$  space group.<sup>6</sup> The unit cell consists of eight formula units. There are two types of Fe positions in this structure. The so-called *A* positions are characterized by tetrahedral oxygen surrounding the Fe ions; the *B* positions have octahedral oxygen coordination. The *A* positions are occupied only by  $\text{Fe}^{+3}$  ions, whereas the *B* positions are occupied with equal probability by  $\text{Fe}^{+2}$  and  $\text{Fe}^{+3}$ .

Magnetite undergoes a first-order transition (the Verwey transition) at  $T_V=120$  K, with changes of crystal structure, latent heat, and a two orders of magnitude decrease of the dc conductivity. This transition was discovered by Verwey<sup>5</sup> in

1939; in his model, the low-temperature phase has the  $\text{Fe}^{+2}$  and  $\text{Fe}^{+3}$  ions at the *B* sites ordered, forming layers of ions of each charge state. Above  $T_V$  there is no long-range order, but short-range order persists. According to neutron measurements,<sup>7</sup> an orthorhombic space groups [either a  $D_{2h}^{11}(Pmca)$  or  $C_{2v}^2(Pmc2_1)$ ] may describe the low-temperature structure.

The Verwey transition has been intensively investigated since its discovery, but remains unexplained. Basically, there are several ideas which partly explain the experimental results, although none is able to give a complete explanation of the transition. This incomplete theory is probably not surprising in a system where the electron-phonon interaction, the electron-electron interaction, and electronic bandwidth are of nearly the same importance. We shall mention some basic ideas which could lead to an understanding of the transition.

Verwey and Haayman<sup>8</sup> originally described this transition as an order-disorder transition. The ordered state is insulating, whereas the disordered state is metallic due to the motion of the extra electron on the *B* positions. Later, Anderson<sup>9</sup> argued that short-range order (SRO) is crucial for understanding the transition and demonstrated that certain SRO configurations are energetically favorable (Anderson's condition). In this picture, long-range order is destroyed above the transition, although short-range order, satisfying Anderson's conditions, persists above the transition. The presence of SRO above the transition was confirmed by neutron measurements. However, there is still a question why an abrupt increase in conductivity is observed in spite of the persistence of SRO above the transition.<sup>10</sup>

Cullen and Callen<sup>11</sup> presented a picture of the transition in which only electron-electron correlations are relevant. It is

assumed that a  $\text{Fe}^{+2}$  ion can be represented as an  $\text{Fe}^{+3}$  ion plus an extra electron. In this case, the physics of  $\text{Fe}_3\text{O}_4$  is just the physics of the interaction of this extra electron with a crystal of  $\text{Fe}^{+3}$  ions. The interaction can be described by the Coulomb nearest-neighbor repulsion and hopping integral for the extra electron. The competition between these two values determines whether an insulator or metal is obtained.

In contrast, Mott,<sup>10,12</sup> Chakraverty,<sup>13</sup> and Yamada<sup>14</sup> emphasized the importance of the electron-phonon interaction. In the Mott<sup>10</sup> picture of the Verwey transition, the charge carriers are either polarons or bipolarons. Above the transition, the system can be described as a Wigner glass, a system where carriers are localized by the disorder-induced random-field potentials. When the temperature is raised, some of the polarons dissociate leading to a hopping type of conductivity.

One should note, however, that an activated conductivity could also be accounted for by the opening of a charge gap. Recent photoemission studies<sup>15</sup> of magnetite indicate a charge gap of 150 meV below  $T_V$ . A recent optical measurement on magnetite<sup>16</sup> found that the main temperature-dependent changes of optical conductivity occur below 1 eV, connected with a gaplike temperature-dependent increase of optical conductivity at 140 meV, followed by a broad polaronic peak at 0.6 eV. The gaplike behavior was attributed to the opening of a charge gap. The authors of Ref. 16 suggested that the charge gap, determined as the onset of the polaronic band in the spectra below the transition, is consistent with the gap value found in photoemission studies. In contrast, we must note that photoemission measures the transitions to the Fermi level, whereas infrared spectroscopy measures an optically allowed transition from one electronic band to another across the Fermi level. This means that the optical gap of 140 meV would suggest a smaller gap, perhaps as small as 70 meV, in photoemission. Moreover, according to Ref. 15, the gap does not close above the transition but rather decreases by only 50 meV, which is not consistent with the analysis of the optical conductivity of Ref. 16. Finally, the activation energy for the dc conductivity should be half the spectroscopic gap value; instead it is reported also to be 140 meV.

In this paper we present the results of systematic temperature-dependant infrared and Raman measurements of magnetite with the main emphasis on lattice dynamics.

### B. Optical phonons in magnetite

Above the Verwey transition temperature,  $T > T_V = 120$  K, magnetite has a cubic-inverse-spinel structure belonging to the space group  $O_h^7(Fd3m)$ . The full unit cell contains 56 atoms but the smallest Bravais cell contains only 14 atoms. As a result, one should expect 42 vibrational modes. Group theory predicts the following modes:

$$A_{1g} + E_g + T_{1g} + 3T_{2g} + 2A_{2u} + 2E_u + 5T_{1u} + 2T_{2u}.$$

The  $T_{1g}$ ,  $A_{2u}$ ,  $E_u$ , and  $T_{2u}$  are silent. Thus, there are five Raman-active modes ( $A_{1g} + E_g + 3T_{2g}$ ) and five infrared-active modes ( $5T_{1u}$ ).

At the Verwey transition, the symmetry of the crystal decreases to orthorhombic. The unit cell doubles along the  $z$

direction and the diagonals of the former cubic unit cell become the faces of the low-temperature unit cell. As mentioned in Ref. 7, it has not been possible to get a complete refinement from the neutron-scattering data. Nevertheless, we can analyze the proposed space groups and compare the results of the group theory analysis with our data. Let us start with  $Pmca$ , which is a nonstandard setting of the  $D_{2h}^{11}, Pbcm$  (No. 57). The unit cell contains 56 atoms, and in this case we cannot reduce the unit cell as was possible for the room-temperature crystal structure. The expected number of modes is 168. Group theory predicts the following modes for this phase:

$$23A_g + 18A_u + 24B_{1g} + 19B_{1u} + 16B_{2g} \\ + 27B_{2u} + 15B_{3g} + 26B_{3u}.$$

The  $A_u$  modes are silent. Thus, there are 78 Raman-active modes ( $23A_g + 24B_{1g} + 16B_{2g} + 15B_{3g}$ ) and 72 infrared-active modes ( $19B_{1u} + 27B_{2u} + 26B_{3u}$ ). It is clear from this analysis that one should expect a dramatic increase in the number of modes in the low-temperature phase. Some of the new modes are the former Brillouin-zone-boundary modes, which become visible because of the unit-cell doubling; others are due to the lifting of degeneracy of former  $T$ - and  $E$ -type modes. Some modes persist over the transition. For instance, the  $A_{1g}$  mode of the cubic phase becomes an  $A_g$  mode of the orthorhombic phase, having the same Raman tensor.

The second proposed symmetry is  $C_{2v}^2, Pmc2_1$  (No. 26). This group does not contain an inversion center, leading to very important consequences for the Raman and infrared spectra. Namely, if magnetite has such a structure below  $T_V$ , both infrared-active- and Raman-active-type modes should be detected by both spectroscopes. Experimentally, this is not the case and we can rule this symmetry out.

The symmetry of the Raman modes can be figured out by their polarization selection rules. The  $A_g$ - and  $E_g$ -type modes have a diagonal Raman tensor so that they are seen only when the polarizations of the incident and scattered light are parallel. In contrast, the  $T_{2g}$ ,  $B_{1g}$ ,  $B_{2g}$ , and  $B_{3g}$  modes have off-diagonal components so that they are observed when the polarizations of the incident and scattered light are perpendicular.

## II. EXPERIMENT

The magnetite single crystals used in this work were grown by a chemical vapor transport technique using stoichiometric  $\text{Fe}_3\text{O}_4$  microcrystalline powder obtained by reduction reaction of ferric oxide ( $\text{Fe}_2\text{O}_3$ ). This procedure yielded near-stoichiometric crystals with a typical size of  $4 \times 4 \times 2$  mm<sup>3</sup>. X-ray diffraction confirmed the spinel-type structure of the crystals. Transport measurements found an abrupt increase in resistance below  $T = 120$  K, characteristic of the Verwey transition. Optical measurements were carried out on the optically smooth surfaces of the as-grown single crystals.

The reflectance was measured in the frequency range of 50–45 000 cm<sup>-1</sup> (6 meV–5.5 eV) at several temperatures between 40 and 300 K. The sample temperature was maintained by mounting the crystal on the cold finger of a He-

flow cryostat. To cover a wide frequency range, we used three optical setups. A Bruker IFS 113V spectrometer was employed for the far-infrared and mid-infrared regions ( $50\text{--}4500\text{ cm}^{-1}$ ;  $6\text{--}550\text{ meV}$ ), and a Perkin Elmer 16U grating spectrometer was used for the near-infrared and visible region ( $3800\text{--}24000\text{ cm}^{-1}$ ;  $0.47\text{--}3\text{ eV}$ ). We observed no temperature dependence of the spectra above  $20\,000\text{ cm}^{-1}$ . Therefore, in order to extend the data to higher frequencies ( $20\,000\text{--}45\,000\text{ cm}^{-1}$ ;  $2.5\text{--}5.5\text{ eV}$ ) we merged the spectrum at a given temperature with the room-temperature reflectance spectrum obtained from a Zeiss grating spectrometer coupled with microscope, and finally in the frequency range above  $45\,000\text{ cm}^{-1}$  we merged our data with the data of Ref. 16.

In order to analyze the optical properties of the sample, we performed Kramers-Kronig transformation of reflectance data. For the temperatures above the transition, we use the Drude-Lorentz model fit in the low-frequency part of the spectrum. Then we calculated the reflectance and used the result for the low-frequency extrapolation. Below the transition, we assume constant dc conductivity at zero frequency as a low-frequency approximation. For the high-frequency approximation, we used a power-law ( $\omega^{-4}$ ) extrapolation.

The polarized Raman scattering experiment was conducted for a wide range of temperatures ( $T=5\text{--}300\text{ K}$ ) using a triple spectrometer equipped with a liquid-nitrogen cooled CCD detector. The  $514.5\text{ nm}$  line of an  $\text{Ar}^+$  laser was used as excitation with nominally  $25\text{ mW}$  incident on the sample. The spectra were taken in the backscattering geometry with the scattered light polarized vertically while the incident light is polarized to select a particular component of the Raman scattering tensor.

### III. RESULTS AND DISCUSSION

#### A. Infrared and Raman-active phonons

We now proceed to analyze the infrared and Raman data keeping in mind all of the above-predicted changes. The infrared reflectance and optical conductivity are shown in Figs. 1 and 2, while the Raman scattering spectra of  $\text{Fe}_3\text{O}_4$  are shown in Fig. 3. Oxygen phonon modes usually have their frequency above  $200\text{ cm}^{-1}$ , whereas vibrations of the heavier iron atoms should be at much smaller frequency. In Figs. 1 and 2, two  $T_{1u}$  oxygen modes are found near  $350\text{ cm}^{-1}$  and  $560\text{ cm}^{-1}$ . These peaks are similar to the optical phonons reported earlier by different groups.<sup>17–21</sup> Four Raman-active phonons are observed at room temperature in Fig. 3. The strongest peak at  $\approx 670\text{ cm}^{-1}$  is either the  $A_{1g}$  or the  $E_g$  mode since it is only present in the parallel polarization geometry ( $XX$ ). Since we expect the  $A_{1g}$  mode to have the highest frequency as it involves the stretching vibrations of the oxygen atoms along the  $\text{Fe}(A)\text{-O}$  bonds, the  $670\text{ cm}^{-1}$  phonon is assigned to the  $A_{1g}$  mode. In Fig. 3, the Raman spectrum in which the incident and scattered light polarizations are perpendicular contains the predicted three  $T_{2g}$  modes at  $193\text{ cm}^{-1}$ ,  $308\text{ cm}^{-1}$ , and  $540\text{ cm}^{-1}$ . Verble<sup>22</sup> made a similar assignment of the Raman-active phonons in  $\text{Fe}_3\text{O}_4$  except for  $193\text{ cm}^{-1}$ , which he did not observe. Instead, he reported that the lowest-frequency  $T_{2g}$  mode is at  $300\text{ cm}^{-1}$  as observed in the spectrum at  $T=77\text{ K}$ . However,

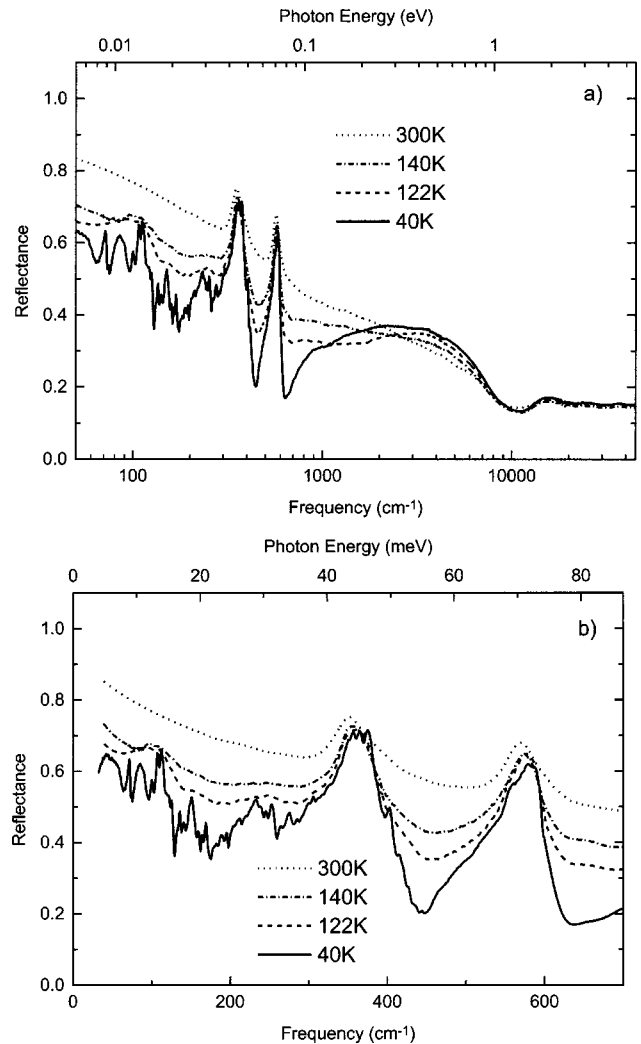


FIG. 1. (a) The reflectance of magnetite in the frequency range from  $50$  to  $45\,000\text{ cm}^{-1}$ . (b) The low-frequency (up to  $700\text{ cm}^{-1}$ ) reflectance of magnetite at temperatures above and below the Verwey transition.

this feature seen by Verble at  $T=77\text{ K}$  ( $<T_V$ ) is related to the structural symmetry breaking that occurs below  $T_V$  as discussed below.

The Verwey transition manifests itself in both infrared and Raman spectra by remarkable changes in the phonon spectrum as the temperature is lowered through  $T_V$ . In the Raman spectrum, one can see at least 17 new modes below  $T_V$ . In addition to the new phonon modes, there is a broad (about  $150\text{ cm}^{-1}$ , full width at half maximum) peak with a maximum at  $350\text{ cm}^{-1}$ . Unfortunately, with so many additional phonon modes it is difficult to judge whether this broad peak is a superposition of phonon modes or a background on which phonon modes are sitting.

There are several additional infrared modes as well. Weak phonon features appear below  $300\text{ cm}^{-1}$  [Figs. 1(b) and 2(b)] in addition to the infrared-active phonons near  $350\text{ cm}^{-1}$  and  $560\text{ cm}^{-1}$ . Similar effects are observed in the Raman spectrum at  $T=5\text{ K}$  as illustrated in Fig. 3. Moreover, the Verwey transition also leads to renormalization of the phonon frequencies and linewidths. The infrared- and Raman-active phonons which persist over the transition were fitted to Lorentzian line shapes in order to obtain their fre-

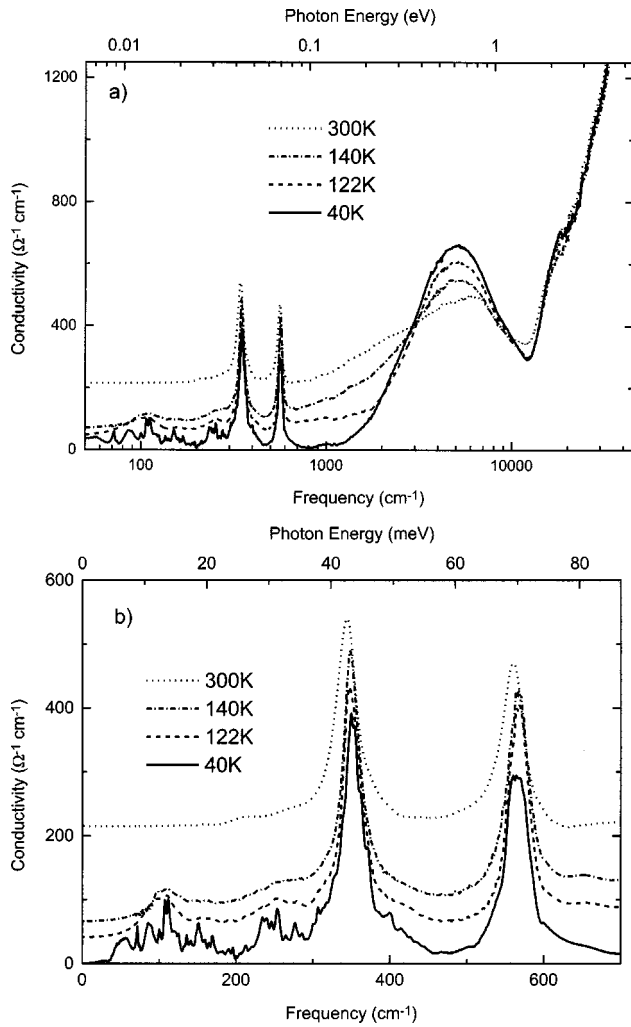


FIG. 2. The optical conductivity of magnetite calculated by the Kramers-Kronig transformation of the reflectance data. (a) shows the optical conductivity below  $45\,000\text{ cm}^{-1}$  and (b) shows the low-frequency optical conductivity (up to  $700\text{ cm}^{-1}$ ) at temperatures above and below the Verwey transition.

quency and linewidths. The results of this analysis are shown in Fig. 4. For the infrared-active phonons at  $350\text{ cm}^{-1}$  and  $560\text{ cm}^{-1}$ , the phonon frequencies increase upon decreasing the temperature but without visible anomalies around  $T_V$ . On the other hand, their linewidths manifest an abrupt increase near  $T_V$ . Additionally, for the  $350$  and  $560\text{ cm}^{-1}$  phonons there is a reproducible fine structure in the reflectance; see Fig. 1(b). At temperatures below the transition, the line shape of the  $350$  and  $560\text{ cm}^{-1}$  phonons cannot be described by a single Lorentzian, which leads to bigger error bars for the linewidth and frequency of these phonons below the transition. See Fig. 4. Note that in contrast to Refs. 13 and 23, within our experimental error we do not observe any soft optical mode.

The observed phonon anomalies can be explained in the following way. Above the transition, most of the phonon modes are highly degenerate modes. When magnetite undergoes the Verwey transition, the crystal symmetry reduces to orthorhombic, lifting the degeneracy of the modes. We suggest that splitting, determined by the degree of distortion associated with the symmetry changes, will not be too large.

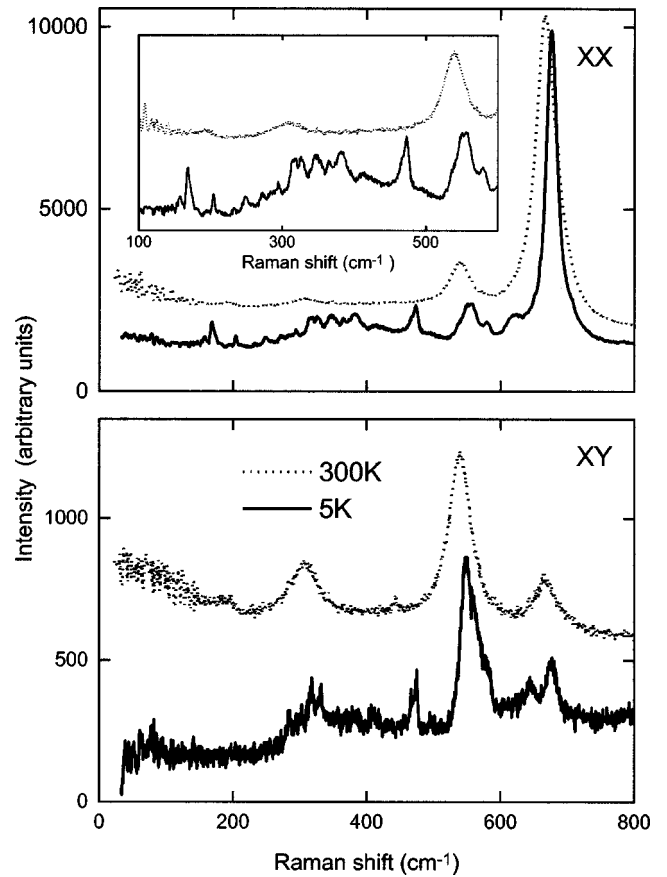


FIG. 3. The Raman spectrum of magnetite at temperatures above and below the Verwey transition. Shown are spectra in the XX geometry and XY geometry. The inset shows the XX spectrum below  $600\text{ cm}^{-1}$ .

According to the neutron data,<sup>7</sup> the Fe-O distances for both A and B sites are generally within the estimated standard deviations for the prototype structure;<sup>24</sup> therefore, one expects the splitting to be small, appearing as a broadening of the modes above the transition. This is what has been observed in our experiment for the two infrared-active modes at  $350$  and  $560\text{ cm}^{-1}$ .

The frequency and linewidth of the Raman-active phonon at  $670\text{ cm}^{-1}$  in Fig. 4 show an abrupt increase in frequency with a concomitant precipitous drop in the linewidth at  $T_V$ . The symmetry of this mode in the cubic phase is  $A_{1g}$ ; it corresponds to the in-phase vibrations of the oxygen ions forming tetrahedra surrounding the Fe ions in the A positions.<sup>22</sup> At the same time, a similar type of displacement for the cubic-orthorhombic structural transition has been found from neutron measurements.<sup>7</sup> Therefore, it is plausible to assume that the  $670\text{ cm}^{-1}$  phonon is directly coupled to the structural displacements at the Verwey transition. This is the reason why this mode is so sensitive to the transition.

## B. Charge dynamics

The electronic features in the midinfrared and higher frequencies are similar to those of Park *et al.*;<sup>16</sup> here we mention briefly the similarities and differences. The optical conductivity (Fig. 2) has a broad temperature-dependent band with a maximum at  $5000\text{ cm}^{-1}$ . The low-frequency (below  $1000\text{ cm}^{-1}$ ) conductivity is strongly decreased at low tem-

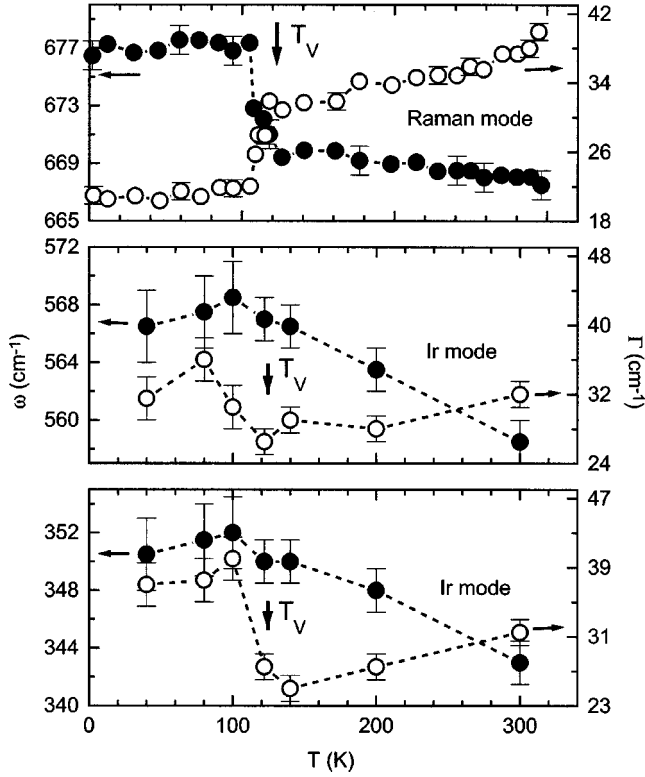


FIG. 4. The frequency (solid circles) and linewidth (opened circles) of the infrared and Raman modes as determined by Lorentzian fits to the data.

peratures, consistent with the temperature dependence of the dc conductivity. From our data, we would estimate the low-temperature charge gap to be at about  $1600 \text{ cm}^{-1}$  (200 meV), a little larger than the 140 meV estimated earlier.<sup>16</sup>

One should note that there are at least two ways to interpret this gaplike feature in the optical conductivity. One can assign such a behavior either to an activated mobility of the form  $\mu_0 \exp(W_H/k_B T)$ , where  $W_H$  is the polaron hopping energy, or to the opening of a charge gap  $2\Delta$ . In the latter case, the carrier concentration will behave like  $n_0 \exp(-\Delta/k_B T)$ , leading to activated conductivity as well.

To analyze the optical conductivity in the polaron picture, we first estimate the oscillator strength or spectral weight in the low-energy region. This quantity is often referred to as the effective number of carriers (per  $\text{Fe}^{+2}$  ion) participating in optical transitions at frequency less than  $\omega$ , defined as<sup>25</sup>

$$\frac{m}{m^*} N_{\text{eff}}(\omega) = \frac{2mV_{\text{cell}}}{\pi e^2 N_{\text{Fe}^{+2}}} \int_0^\omega \sigma_1(\omega') d\omega',$$

where  $m$  is the free-electron mass,  $m^*$  is the effective mass of the carriers,  $V_{\text{cell}}$  is the unit-cell volume, and  $N_{\text{Fe}^{+2}}$  is the number of  $\text{Fe}^{+2}$  ions per unit cell. Figure 5 shows the result of this calculation at four temperatures. Using the definition of  $N_{\text{eff}}$ , we can try to estimate the effective mass of the carriers. Let us assume that  $N_{\text{eff}}(1600 \text{ cm}^{-1})$  is purely due to the free-carrier optical conductivity, corresponding to one mobile carrier per  $\text{Fe}^{+2}$  ion. Then, the value of  $m/m^* N_{\text{eff}}(1600 \text{ cm}^{-1}, 300 \text{ K}) \approx 0.01$ , gives  $m^* \approx 100m$ .

We compare this number to the effective mass from the Mott equation:<sup>10</sup>

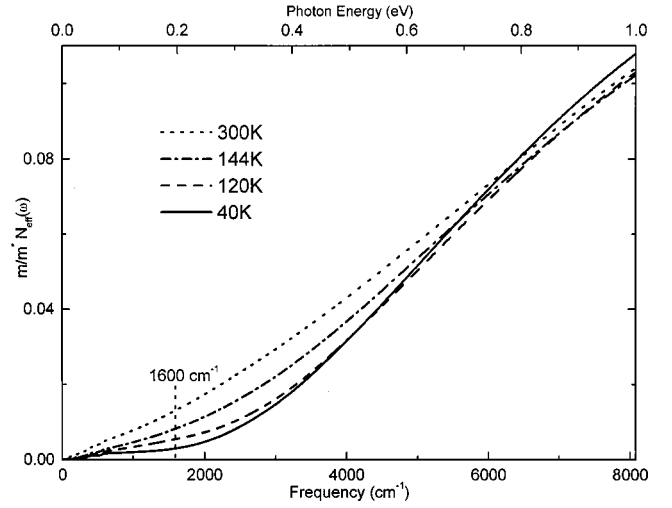


FIG. 5. The effective number of carriers participating in optical transitions at frequencies below  $\omega$  [ $N_{\text{eff}}(\omega)$ ] versus  $\omega$  at temperatures above and below the Verwey transition.

$$m^* \approx 5m \exp(W_H / \frac{1}{2} \hbar \omega),$$

where  $\hbar \omega$  is the zero-point phonon energy. We can estimate  $W_H$  from the polaron peak position: namely, the peak position ( $\approx 5000 \text{ cm}^{-1}$ ) gives us  $2W_B$ , where  $W_B$  is the polaron binding energy. In the simple model of an electron jumping between two molecules,<sup>12</sup> the hopping energy can be estimated as  $W_H \approx 1/2 W_B$ , yielding  $W_H = 1250 \text{ cm}^{-1}$ . The zero-point phonon energy can be taken to be the frequency of the highest-energy optical phonon,  $670 \text{ cm}^{-1}$ . These values give  $m^* \approx 200m$ , the same order of magnitude that we obtained from  $N_{\text{eff}}$ . Note that the Mott formula contains an exponent which is very sensitive to both values of  $W_H$  and  $\frac{1}{2} \hbar \omega$ , therefore the fact that we have got the right order of magnitude for the effective mass is consistent with the idea of a polaron mechanism of conductivity in magnetite.

#### IV. CONCLUSIONS

We have presented results for infrared and Raman measurements of magnetite. Both Raman and infrared spectroscopic techniques observed phonon anomalies at  $T_V$  which are attributed to the symmetry and structural changes below  $T_V$ . We are able to rule out a structure lacking inversion symmetry.

Our optical conductivity data seem to fit to the polaronic picture of the Verwey transition. At the temperatures below  $T_V$ , carriers are localized polarons and we have a strong polaron peak at  $\approx 5000 \text{ cm}^{-1}$  and a gaplike decrease of optical conductivity below  $1000 \text{ cm}^{-1}$ . All polarons are bound and the position of the polaron peak occurs at twice the binding energy.

At temperatures above the transition, some carriers are delocalized, leading to the removal of oscillator strength from the  $5000 \text{ cm}^{-1}$  peak, broadening, and an increase of the low-frequency conductivity, consistent with the previous observations of Park *et al.*<sup>15</sup>

We emphasize that it is difficult to separate effects of the filling of the charge gap or the activated increase of mobility.

However, no matter what is causing it, the low-frequency optical conductivity follows the dc conductivity.

The effective mass of the carriers estimated from the optical conductivity gives a value of  $\approx 100m$ , close to that predicted by Mott in the framework of the polaron model of the Verwey transition. All these observations strongly indicate the importance of lattice dynamics effects, favoring the polaronic picture of the Verwey transition.

## ACKNOWLEDGMENTS

Work at Florida was supported by NSF Grant No. DMR-9705108. L.V.G. acknowledges Dr. E. Ya. Sherman for a critical discussion of the manuscript. D.B.R. acknowledges Dr. Raju Datla for his interest in and support of the Raman work at NIST. H.B. wishes to express appreciation to Dr. J. Lammer for fruitful discussions.

- 
- <sup>1</sup>J.D. Axe *et al.*, Phys. Rev. Lett. **62**, 2751 (1989).  
<sup>2</sup>J.M. Tranquada *et al.*, Phys. Rev. Lett. **78**, 338 (1997).  
<sup>3</sup>M. Fischer, P. Lemmens, G. Els, G. Güntherodt, E. Sherman, E. Morre, C. Geibel, and F. Steglich (unpublished).  
<sup>4</sup>S. Mori, C.H. Chen, and S.-W. Cheong, Nature (London) **392**, 473 (1998).  
<sup>5</sup>E.J.W. Verwey, Nature (London) **144**, 327 (1939).  
<sup>6</sup>W.H. Bragg, Philos. Mag. **30**, 305 (1915).  
<sup>7</sup>M. Iizumi, T.F. Koetzle, G. Shirane, S. Chikazumi, M. Matsui, and S. Todo, Acta Crystallogr., Sect. B: Struct. Sci. **39**, 2121 (1983).  
<sup>8</sup>E.J.W. Verwey and P.W. Haayman, Physica (Amsterdam) **8**, 979 (1941).  
<sup>9</sup>P.W. Anderson, Phys. Rev. **102**, 1008 (1956).  
<sup>10</sup>N.F. Mott, Philos. Mag. B **42**, 327 (1980).  
<sup>11</sup>J.R. Cullen and E.R. Callen, J. Appl. Phys. **41**, 879 (1970).  
<sup>12</sup>I.G. Austin and N.F. Mott, Adv. Phys. **18**, 41 (1969).  
<sup>13</sup>B.K. Chakraverty, Solid State Commun. **15**, 1271 (1974).  
<sup>14</sup>Y. Yamada, Philos. Mag. B **42**, 377 (1980).  
<sup>15</sup>J.-H. Park, L.H. Tjeng, J.W. Allen, P. Metcalf, and C.T. Chen, Phys. Rev. B **55**, 12 813 (1997).  
<sup>16</sup>S.K. Park, T. Ishikawa, and Y. Tokura, Phys. Rev. B **58**, 3717 (1998).  
<sup>17</sup>T.R. Hart, H. Temkin, and S.B. Adams, in *Proceedings of the Third International Conference on Light Scattering in Solids*, edited by M.Balkanski, R.C.C. Leite, and S.P.S. Porto (Flammarion, Paris, 1976), p. 254.  
<sup>18</sup>A. Shlegel, S.F. Alvarado, and P. Wachter, J. Phys. C **12**, 1157 (1979).  
<sup>19</sup>A. Shlegel and P. Wachter, J. Phys. (Paris), **41**, 19 (1980).  
<sup>20</sup>L. Degiorgi, I. Blatter-Mörke, and P. Wachter, Phys. Rev. B **35**, 5421 (1987).  
<sup>21</sup>L. Degiorgi, P. Wachter, and D. Ihle, Phys. Rev. B **35**, 9259 (1987).  
<sup>22</sup>J.L. Verble, Phys. Rev. B **9**, 5236 (1974).  
<sup>23</sup>G. Galeczki, R.A. Buckwald, and A.A. Hirsch, Solid State Commun. **23**, 201 (1977).  
<sup>24</sup>Z. Zgang and S. Satpathy, Phys. Rev. B **44**, 13 319 (1991).  
<sup>25</sup>F. Wooten, in *Optical Properties of Solids* (Academic Press, New York, 1972).